LA-6171-PR
Progress Report

UC-95b
Issued: December 1975

USERDA Division of Electric Energy Systems DC Superconducting Power Transmission Line Project at LASL

April 1—June 30, 1975

Compiled by

W. E. Keller
R. D. Taylor

los alamos
scientific laboratory
of the University of California
LOS ALAMOS, NEW MEXICO 87545

An Affirmative Action/Equal Opportunity Employer

UNITED STATES
ENERGY RESEARCH AND DEVELOPMENT ADMINISTRATION
CONTRACT W-7405-ENG. 36

The four most recent reports in this series, unclassified, are LA-5787-PR, LA-5851-PR, LA-5972-PR, and LA-6053-PR.

In the interest of prompt distribution, this report was not edited by the Technical Information staff.

Work supported by the USERDA Division of Electric Energy Systems.

Printed in the United States of America. Available from
National Technical Information Service
U.S. Department of Commerce
5285 Port Royal Road
Springfield, VA 22151
Price: Printed Copy $5.00 Microfiche $2.25

USERDA Division of Electric Energy Systems

DC Superconducting Power Transmission Line Project at LASL

April 1 — June 30, 1975

Compiled by

W. E. Keller and R. D. Taylor

ABSTRACT

The ~~tenth~~ progress report of the Los Alamos Scientific Laboratory dc Superconducting Power Transmission Line (SPTL) Development Project covers the period April 1 to June 30, 1975. A number of line configurations, including a high voltage dc SPTL design, are examined from a cryoengineering point of view. New calculations on the cryostabilization of the superconductors are presented. Measurements of the critical current on several new superconductors and on a 20-m, well-stabilized Nb_3Sn tape are reported. Acoustical emission is being evaluated as a new technique to predetermine damage to Nb_3Sn conductors during cable fabrication.

I. INTRODUCTION AND SUMMARY

The Los Alamos Scientific Laboratory (LASL) is developing direct current superconducting cables for transmitting electrical power at nearly 100% efficiency. The national trend toward siting large generating stations and complexes (power parks) far from load centers — sometimes hundreds of kilometers — indicates the real and increasing need for efficient transmission of large blocks of power. Preliminary studies have already strongly suggested that a dc superconducting power transmission line (dc SPTL) would offer overall economic, operating, and environmental advantages for this service when compared with conventional methods of transmission. Although it was originally believed that these advantages would accrue only for power loads of about 10 GVA and larger, LASL investigations of small-diameter line designs have suggested a reduction to about 2-3 GVA as an estimate for the minimum economically competitive load size for the dc SPTL.

The small-diameter line concept is being developed for a prototype test of a section of a 5-GVA power transmission line.

This document is the tenth progress report of the LASL dc SPTL Project and covers the period from April 1 to June 30, 1975. It describes the continuation of work directed toward the applications mentioned above and discussed in previous reports, denoted in this report as PR-1 to PR-9. Recent reports in this series (LA-5787-PR, LA-5851-PR, LA-5972-PR, and LA-6053-PR) are available from LASL or the National Technical Information Service, Springfield, VA, 22151.

Short sample critical currents of several different types of developmental samples are reported in Sec. II. A discussion and first results of the new program to measure ripple and ac losses in superconductors are presented. Calculations of the maximum thickness of Nb_3Sn layers for adiabatic stability at various temperatures and the maximum surface current density I' for "optimized" Nb_3Sn layers have been refined. The influence on I' of a temperature gradient along the conductor is examined.

Measurements of critical current as a function of temperature for a 20-m long, well-stabilized sample of Nb_3Sn tape are reported in Sec. III.

A high-voltage dc SPTL concept is considered in Sec. IV. The influence of several cryoengineering parameters on the performance and cost of various line-refrigerator concepts is also given.

A preliminary investigation of acoustical emission as a technique useful in assessing damage to brittle A-15 superconductors is described in Sec. V. New developments in producing high T_c materials based on Nb_3Ge are also reported.

II. SHORT SAMPLE TESTS

II-1. Critical Current Measurements

II-1.1 Nb_3Ge

As reported in PR-9, the LASL Nb_3Ge samples produced by the CVD (chemical vapor deposition) process were found to contain O_2. Efforts have been directed to reducing or eliminating the O_2 content and to correlating the O_2 content with other physical properties of the material. Some correlation between the presence of oxygen in a sample and the quality of its x-ray spectrum has been observed; perhaps there may also be a dependence of the critical current density and/or dJ_c/dT on the amount of O_2 in the sample. To test this conjecture we have measured J_c and dJ_c/dT for six samples with varying amounts of oxygen and one sample with 4.8 at% Si. The results are shown in Fig. 1. There are too few data to draw any definite conclusions. However peaks in J_c and dJ_c/dT appear at approximately 4 at% O_2 and the x-ray structural quality factor (defined as the number of resolved doublets in the x-ray pattern) peaks near 5 at% O_2, suggesting that the two effects may be correlated. If the correlation is found to be more generally true, x-ray examination of Nb_3Ge samples containing other types of impurities will assist in optimizing the J_c and dJ_c/dT characteristics of Nb_3Ge.

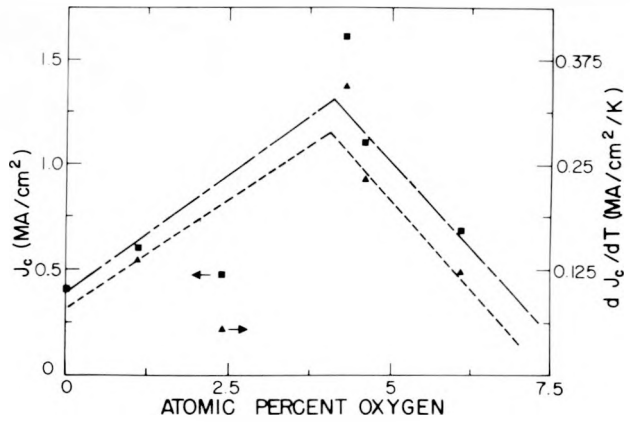

Fig. 1. The effect of oxygen content in Nb_3Ge on J_c and dJ_c/dT at 14 K. Fig. 18 of PR-9 shows the effect of oxygen content on the x-ray structure quality. Maxima occur at approximately 4 at%.

II-1.2 Tsuei-type Superconducting Wire

A LASL sample of 90% Cu – 10% Nb was tested for superconductivity at 4 K. The wire (5.5-m long and 0.127-mm diam) was wound noninductively on a 2.54-cm-diam spool with current and voltage connections made at each end. The sample carried 10.5 A with a voltage drop of less than 0.1 μV. This corresponds to a resistivity of less than 2.2×10^{-15} Ω-cm. As the current was increased above 10.5 A, the voltage rapidly increased. In this dissipative regime the sample was still stable and showed no signs of flux jumps. As the current was reduced below 10.5 A, the voltage dropped below the limit of detection. This is one of the longest samples of Tsuei-type wire tested and shows the integrity of such wire.

II-1.2 Short Sample Test of Test-Bed Sample

The critical current I_c of a 1.27-cm-wide Nb_3Sn tape, clad on each side with 0.0127-cm-thick copper, (Intermagnetics General Corp. Type 9253) was measured down to 16 K. Below 16 K the sample could not be driven normal by the 500 A available from the power supply. A second sample of this tape was soldered to a long 0.32- x 1.27-cm copper bar to provide mechanical, cryogenic, and electrical stabilization required for experiments in the 20-m test bed. At temperatures below T_c a section of this copper-supported sample carried about the same critical current as determined for the tape alone. The long sample, measured in the test bed and discussed further in Sec. III, carried about 80% of the short sample current at a temperature near 16 K.

Another section of this test-bed sample was tested at 4 K using the dc transformer technique. The I_c at 4 K was determined to be 6.9 kA, which agrees well with the result determined in the 20-m test bed (Sec. III).

II-1.4 Multifilamentary Nb_3Sn Cables

One of the possible conductor designs for a dc SPTL is a multifilamentary (MF) Nb_3Sn cable. Such a cable might be made in long continuous lengths which could be pulled into a prepared cryogenic envelope made up of shorter modules. It would be a relatively flexible conductor, and the thermal contraction problem would be more tractable than with most other conductor geometries. Because of these and other possible advantages, tests on MF wire have been instigated as commercial materials became available. Some results have been reported earlier; new results on several cables fabricated from MF wire manufactured by AERE Harwell are presented here.

Two of the cables, differing only in the form of the copper center core, were formed by wrapping six unreacted Harwell MF wires around either a solid or a stranded copper core with a pitch of approximately 2 turns per cm. A third cable consisted of three twisted MF wires with no copper stabilization. The three fabricated cables were heat treated at 750°C for 60 h and then impregnated with In-Sn solder.

Critical current density vs temperature curves for the three cables are shown in Fig. 2. For comparison, the results of a single wire which had received a similar heat treatment are shown. All of the cables had a critical current density J_c as large or larger than the single wire. The J_c of the twisted cable was greater than that of the wrapped cable, but no great significance is placed on this result at present because sample-to-sample variations may account for the difference.

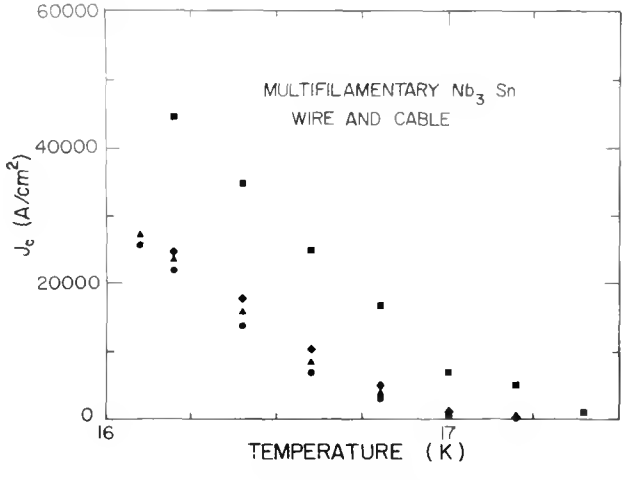

Fig. 2. Critical current density as a function of temperature for four cables made from 0.61-mm-diam multifilamentary Nb_3Sn wire (manufactured by AERE Harwell Ltd). The cable configurations are indicated by: ● single wire, ◆ six wires wrapped on a solid copper core, ▲ six wires wrapped on a stranded copper core, and ■ three twisted wires. Current densities are based on the total wire cross section.

The added copper stabilization in the wrapped conductors consisted of either a solid 1.6-mm-diam wire or seven strands of 0.8-mm-diam wire and was deemed adequate. No flux jumps were observed, and the I-V curve was reversible through the normal-superconducting transition. The twisted cable, which had no added copper stabilization, exhibited a very sharp nonreversible jump from the superconducting to normal state; nevertheless, J_c for this cable appeared to be higher than that for the copper stabilized cable. Degradation of the reacted cables due to bending and to normal handling has not been investigated.

II-1.5 Data Acquisition System

Obtaining critical current data as a function of temperature has been a rather slow, tedious task because the measurements have been taken manually. At each temperature the current through the sample was increased until a small voltage appeared across the sample; the critical current was determined from an X-Y recorder trace of I vs V where voltages less than a μV could be discerned. The pressure in the cryostat was controlled by a manostat, and the temperature was determined from the vapor pressure of the cryogen.

This procedure has now been semiautomated through the use of a data acquisition system (Hewlett Packard Model 3050A) which uses a BASIC program to control the experiment. The system is shown in Fig. 3. Once the sample is in place and the liquid He or liquid H_2 transferred into the cryostat, an I_c vs T profile for the sample is obtained automatically. At a number of fixed temperatures, starting at an initial temperature slightly above T_c for the sample, the sample current is increased until a voltage of approximately 0.1 μV is observed (this discrimination voltage can be varied slightly depending on the noise level of the system). At this point the current and temperature are plotted, printed, and recorded

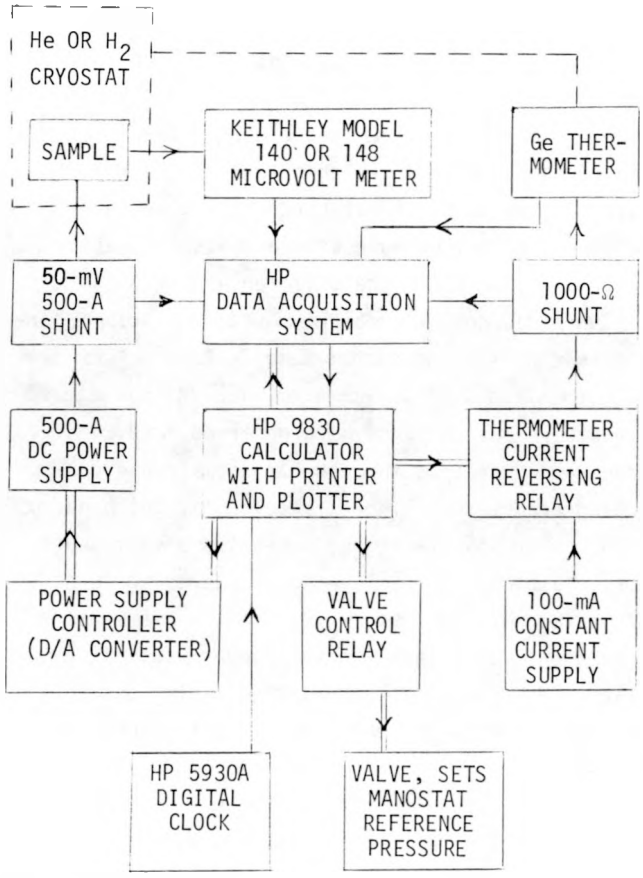

Fig. 3. Block diagram of data acquisition system for automatically measuring the critical current of a superconductor as a function of temperature between 21 K and 13.8 K and at 4 K. The critical current is defined as that current which produces a 0.1-μV drop across a 1-cm length of the sample. The Ge thermometer was mounted on the sample holder. Signal channels are indicated by single lines. Double lines indicate control functions.

on magnetic tape. The system then automatically lowers the temperature about 0.1 K by interactively reducing the manostat reference pressure. After equilibration at the new temperature the critical current is determined as before. The cycle is repeated with little operator attention except for the need to measure the level of the refrigerant bath. At each step, the temperature is determined from a calibrated Ge thermometer.

II-2. AC Loss Measurements

II-2.1 General

As indicated in previous reports (PR-8 and PR-9), the purpose of undertaking ac loss measurements is to be able to assess the ripple losses which may be associated with a dc SPTL. To this end, we first must have the capability of reliably measuring ac losses in superconductors in the absence of a dc bias. Considerable effort has been expended this quarter in identifying and eliminating sources of spurious signals in the ac loss apparatus, and we now believe accurate determinations of ac losses are possible. Consequently, measurements of the ac power loss in a Nb rod have been made as a function of both amplitude and frequency of an applied ac magnetic field. Not surprisingly, the results are in basic agreement with data published in the literature, but they are somewhat higher because the sample surface was macroscopically rough. The standard electronic technique which we have chosen for the loss measurement also makes it possible to study the voltage waveform associated with the hysteretic penetration of flux into the superconductor. This information is valuable for comparison with critical state models.

II-2.2 Electronic Technique Considerations

The electronic technique for measuring ac losses in tubular superconducting samples was outlined in the preceding progress report (PR-9). The design consists of a liquid-helium-immersed copper solenoid, which applies an alternating axial magnetic field to the sample surface. The solenoid has a resistance of nearly 1 Ω at 4 K and produces approximately 585 Oe/A at its center. Thus fields considerably larger than H_{c1} for either Nb, Nb_3Sn or Nb_3Ge are readily attainable with acceptable power dissipation in the helium bath. The loss signal is detected by a single-layer pick-up coil having 126 turns of 3-mil (76-μm) wire wound directly on the surface of the sample. This coil is situated near the center of the ac solenoid, which is homogeneous to ± 1% over the central two centimeters.

Flux linkages in the pick-up coil due to the finite size of the wire also produce an inductive signal two to four orders of magnitude greater than the ac loss signal. In order to eliminate this undesirable signal one typically uses a reference coil to produce an inductive signal which can be added to the pick-up coil signal. In this way the unwanted inductive signal in the pick-up coil can be bucked out leaving only the loss signal. Because the inductive signal is so much larger than the loss signal, any relative phase shift greater than 0.0001°

to 0.01° between the reference coil and pick-up coil signals will introduce a large error into the determination of the ac loss voltage.

In order to avoid the complication of small phase shift errors, we initially adopted a compensation scheme similar to one first proposed at Holifield National Lab.[1] With this technique, compensation is attained by mechanical adjustment of a coil in series opposition with the pick-up coil, which is situated completely in the fringing field of the ac solenoid. This method has the advantage of compensating the large inductive signal prior to application of the signal to the external electronics where phase shifts can occur. Measurements using this technique have resulted in a power loss with an appreciable nonhysteretic f^2 component.

A thorough investigation of possible sources of spurious f^2 eddy-current-like signals, carried out using a dummy phenolic sample, allowed us to conclude that the largely asymmetric coil system first employed resulted in a significant nonhysteretic pick-up signal. This was possibly due to eddy currents generated both in the surrounding copper solenoid and in the pick-up coil itself and to coupling with metallic objects external to the dewar. Significantly, when the solenoid was operated in a liquid nitrogen bath, these f^2 "losses" diminished, presumably as a result of the increased resistance (20 x) in the copper solenoid and pick-up coil. We were able to reduce further the f^2 contribution by winding exactly balanced coils on the phenolic rod. Therefore, it is important that both the pick-up and compensating coils "see" very nearly the same field. In addition, we found that common mode voltages generated by a large impedance mismatch between the pick-up coil arrangement and the signal pre-amplifier could result in a substantial error in determining the proper ac loss voltage.

As a result of these investigations, we have developed a compensation technique that reduces most of the difficulties mentioned above. Here, the compensation coil is wound directly over the pick-up coil and in series opposition to it (see Fig. 4). Both the pick-up and compensating coils are wound from the same unbroken length of wire, which is a high-resistance (3.3 Ω/cm) W-8% Pt alloy wire. The use of a high-resistance wire for the pick-up coil not only reduces eddy current losses

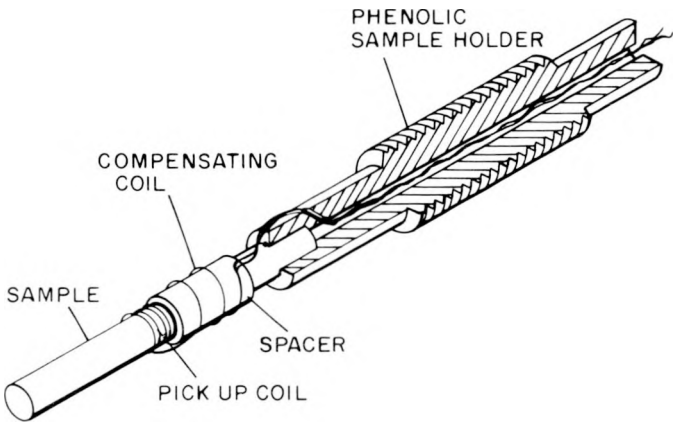

Fig. 4. Pick-up and compensating coil geometry for ac loss measurements.

which may be present in it but also presents a much better impedance match to the external circuitry. In order to enclose the same amount of flux in each coil and maintain a significantly different turns ratio, the compensating coil is spaced away from the pick-up coil by a nylon cylinder. With the geometry shown in Fig. 4, the turns ratio of compensating-to-pick-up coil is 1:16. As can be seen, approximately 70% of the compensating coil is wound directly over the central region of the pick-up coil. The remaining portion of the compensating coil is wound so that it barely extends into the fringing region of the copper solenoid. Thus the two coils are very nearly symmetrically located in the applied field. Compensation is achieved by a small mechanical adjustment of the sample pick-up coil / compensating coil combination so that slightly more or less flux links with the upper section of the compensating coil, while the pick-up coil and the major portion of the compensating coil remain in the uniform field region of the solenoid.

The loss signal is measured using a lock-in amplifier. The signal from the pick-up coil arrangement is first amplified and then applied to the signal channel of the lock-in detector. The reference channel is driven by a signal in phase with the solenoid current. The proper phase setting of the detector is determined by mechanically unbalancing the pick-up coil arrangement so that a very large inductive signal is applied to the lock-in signal channel. This signal is almost exactly 90° out of phase with the reference channel so that the lock-in

phase can be set appropriately. Compensation is determined by requiring that this signal out of phase with the current be a minimum. The ac loss voltage is then that signal that remains and is in phase with the current at the fundamental frequency. This technique is relatively insensitive to errors as large as ± 10° in the exact setting of the phase.

II-2.3 Measured ac Losses

Using the technique outlined, ac power losses have been measured on a Nb rod as a function of both applied field amplitude and frequency. Representative results for the field dependence are shown in Fig. 5. The power loss at 50 Hz exhibits a field amplitude dependence of H^4 over the entire range of applied fields. The absence of any H_{c1} effects is to be expected for this as-machined sample which has a macroscopically irregular surface. As pointed out by Buchhold,[2] surface roughness causes local premature flux entry in regions of high demagnetization factor, thus masking any bulk H_{c1} effects.

As indicated earlier, the electronic technique of measuring ac power losses also enables us to view the associated loss voltage waveform. Such loss waveforms have been calculated based upon various critical state models.[3] Shown in Fig. 6 is a typical loss waveform observed for the Nb rod. The

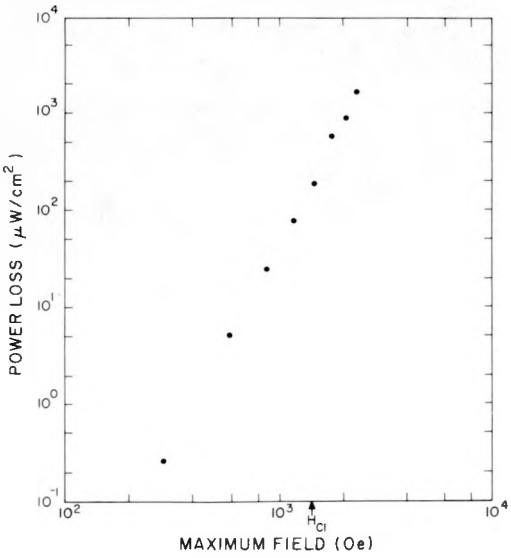

Fig. 5. Measured power loss in a Nb rod as a function of maximum applied field with the frequency fixed at 50 Hz. The field dependence exhibited is approximately H^4.

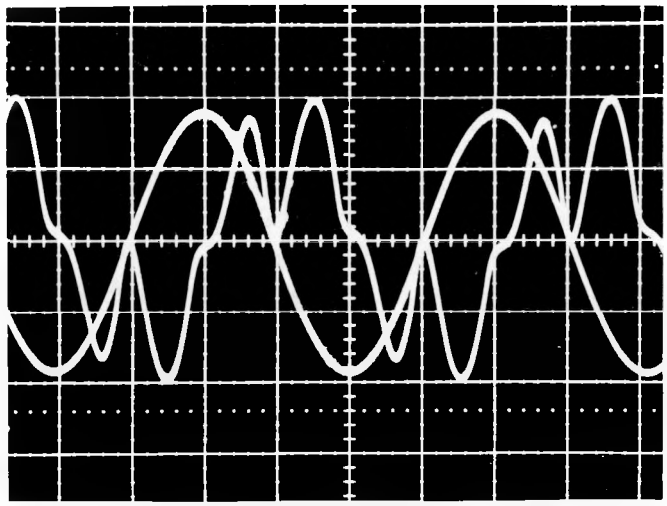

Fig. 6. Loss voltage waveform for a Nb rod and superimposed sinusoidal current waveform as a function of time. Vertical axis for the loss voltage is 50 μV/div. Maximum current is 2 A. Horizontal axis 50 ms/div. See text for discussion.

frequency in this case is 50 Hz. Characteristic of all critical state model predictions is a zero loss voltage at extrema in the applied field. This expectation is confirmed in Fig. 6. It can also be seen that the loss voltage is zero when the applied field is zero, a condition possible only in critical state models which assume J_c to be inversely proportional to some power of the applied field. In particular, the Kim critical state model predicts $J_c \propto 1/B$ and an H^4 field dependence for the power loss.[3] Therefore, it appears that both Figs. 5 and 6 reflect the existence of a Kim-like critical state in this Nb rod. However, in light of recent experiments which cast some doubt on the existence of a critical state,[4] we can not rule out the possibility of some other mechanism being responsible for such behavior. It should also be noted that no surface screening effects, such as H_{c1} or ΔH,[3] are observed in the loss waveform for this sample, in agreement with the field dependence results.

The frequency dependence of the ac power loss was measured as well. Fig. 7 is an example of such a measurement taken at a constant amplitude applied field of 867 Oe, which corresponds to a linear current density of roughly 500 A/cm in the superconductor. The plot is very nearly linear, indicative of hysteresis. As a check on the

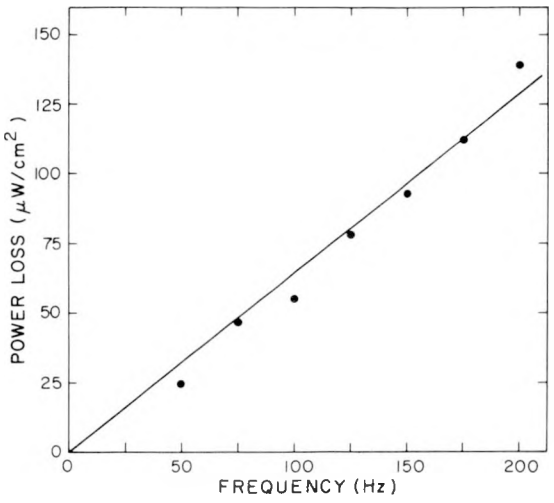

Fig. 7. Measured power loss in a Nb rod as a function of frequency for a fixed field of 867 Oe. The solid line is a linear least squares fit to the data.

presence of a possible nonhysteretic component, plots of energy/cycle vs frequency were made for a variety of exciting field amplitudes. Such plots are appreciably more sensitive to the existence of any f^2 components. It was found that an f^2 contribution to the measured power loss was present in spite of the many precautions taken to avoid it. However, this contribution was a significant fraction of the total power loss only at the lowest fields and highest frequencies.

Our present feeling is that these nonhysteretic contributions are spurious, the result of fields produced by eddy currents in the copper solenoid which couple differentially to the pick-up and compensation coils. Further variation of coil configurations will be employed to determine this point.

Our immediate plans call for the measurement of ac losses in the Nb_3Ge material being prepared by the CVD process at LASL. The specimens to be measured will be in the form of 10-30-μm coatings of Nb_3Ge on the outside of a 6-mm-diam substrate rod. AC losses will be correlated with dc critical current measurements taken on the same specimens.

II-2.4 References

1. Quarterly Report, Cryogenic Power Transmission Technology, ORNL-TM-4824, July 1 – Sept. 30, 1974.
2. T. A. Buchhold, Cryogenics 3, 141 (1963).
3. W. I. Dunn and P. Hlawiczka, J. Phys. D 1, 1469 (1968).
4. R. W. Rollins, Heinz Küpfer, and Wolfgang Gey, J. Appl. Phys. 45, 5392 (1974).

II-3. Stabilization of Superconductors

II-3.1 Adiabatic Stability Limits of Thin Films

The adiabatic stability criteria for thin superconducting films on the surface of a tube (discussed in previous progress reports, cf Fig. 12 of PR-9) can be presented in a more convenient form as shown in Fig. 8. We now simply plot the maximum permitted linear current density (in A/cm of tube circumference) as a function of the minimum transmission line temperature, T_{MIN}, and introduce as a parameter the maximum expected temperature rise, ΔT, along the line. It is assumed, of course, that the film thickness has been matched to the chosen value of T_{MIN} according to Fig. 9, a criterion discussed in PR-7.

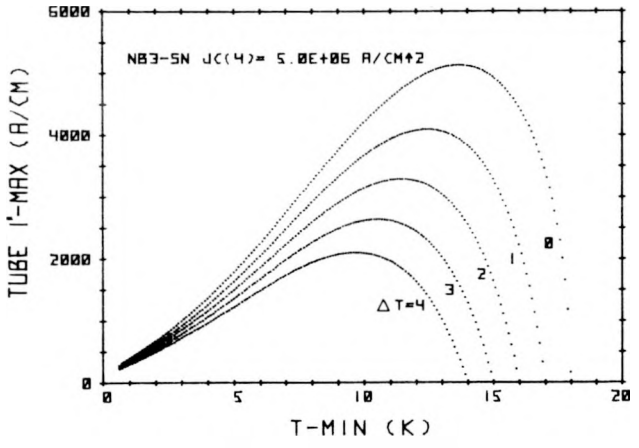

Fig. 8. Maximum linear current density, I'_{MAX} (in A/cm) for an adiabatically stable superconducting film on the surface of a tube, plotted against minimum operating temperature, T_{MIN}, with the temperature rise, ΔT, as a parameter. The curves shown are for "standard" Nb_3Sn where the self-field critical current density at 4 K is taken to be 5×10^6 A/cm^2.

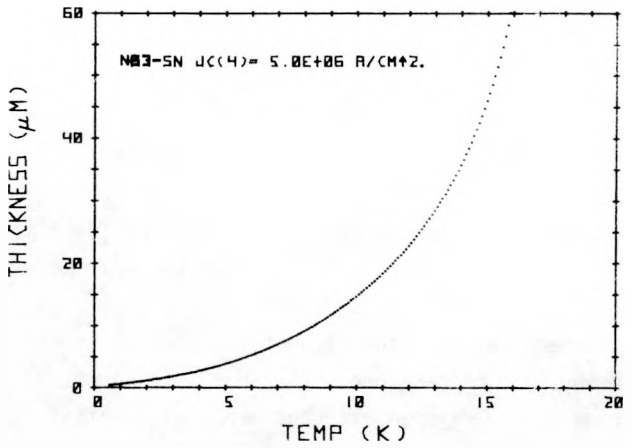

Fig. 9. Maximum possible thickness (in μm) for adiabatically stable "standard" Nb_3Sn film as a function of temperature (T_{MIN} in Fig. 8).

II-3.2 Cryostability Experiment

II-3.2.1 Apparatus

Apparatus for the cryostability experiment (growth or decay of a normal zone) discussed in PR-8 and PR-9 has been constructed and is now being assembled. The modular apparatus, essentially a blow-down cryostat and miniature transmission line, is shown schematically in Fig. 10. A 4-liter high-pressure container with liquid helium can be pressurized up to 20 atm. The supercritical fluid can flow at rates up to 1 g/s through a 0.8-m-long heat exchanger in a copper block at a temperature of up to 20 K; temperatures are controlled by a thermometer, a 100 W-heater, and associated electronics. Following the heat exchanger is a flow control valve, a 100-or 1500-A counterflow current lead, a 1-m-long test section (which can be lengthened if necessary), the other current lead, and a heat exchanger to handle the main gas flow. The test section also has provision for injecting a normalizing current pulse of variable duration and energy over a known length of the conductor sample.

The remainder of the apparatus consists of thermometers, pressure and backpressure regulators, heat exchangers and flow meters for accurate mass-flow determination, and a 1500-A totally-battery-operated power supply.

II-3.2.2 Associated Data

It now appears that in addition to its primary use in cryostability tests the apparatus

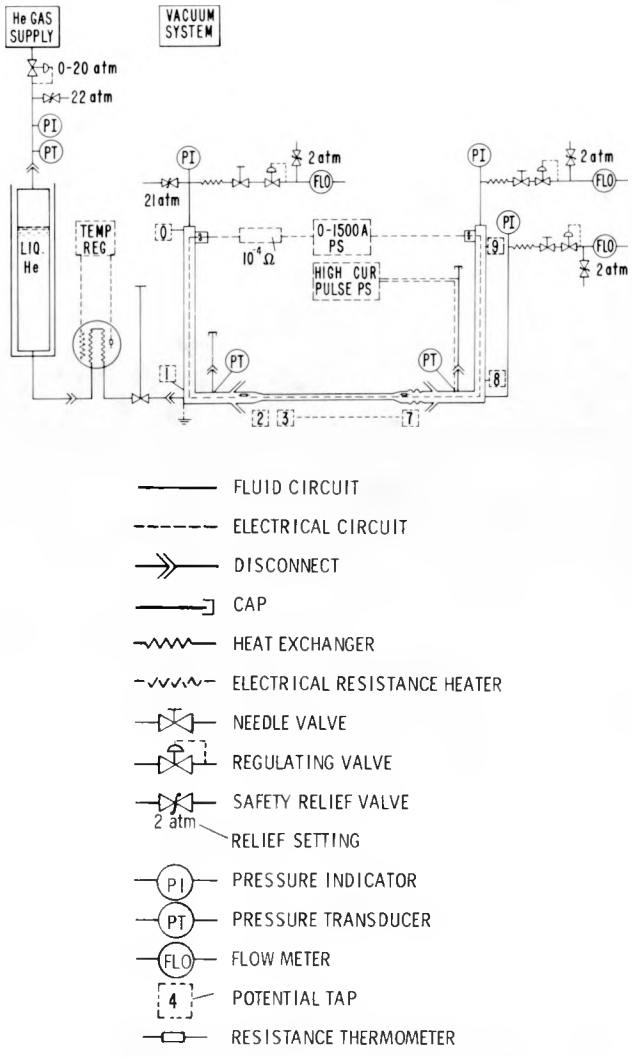

Fig. 10. Schematic of cryostat for cryostability measurements over extended range of temperature, pressure, cryogen flow, and heat transfer conditions. Special symbols are identified above.

should also provide useful information on: 1) variable temperature short sample critical current measurements over the entire range of 4 to 20 K; 2) experimental verification of heat transfer coefficients and friction factors over wide temperature, pressure, and flow ranges and for Reynolds numbers of up to 10^5; and 3) evaluation of cryogenic current leads that are cooled by a controlled flow of cold pressurized gas rather than in the conventional manner by boil-off from a liquid helium bath. There is little information available on the performance of leads which use only cold gas, and such leads will likely be used on the dc SPTL.

II-3.2.3 Power Supply

The design of ripple-free, battery-operated power supplies, based on the power control elements of the 50-kA battery supply for the 20-m test facility but with different control circuitry, was mentioned in PR-9. One supply has been completed and has been tested on a short circuit load. It will be used in the cryostability experiments. Current ramp rates of 0.1 to 5000 A/s in 15 increments have been made available with a hold capability at any chosen current. A second unit is under construction.

III. 20-M TEST FACILITY FOR SUPERCONDUCTING POWER TRANSMISSION STUDIES

III-1. Braided NbTi Sample

The installation and initial tests on a NbTi braided wire sample were described in Sec. III-4 of PR-9. It was not possible at that time to obtain meaningful measurements on the electrical characteristics of this sample because the bolted joint blocks between the sample and the potheads would overheat at currents well below the critical current $I_c(T)$ of the sample. During the first part of this report period, several necessary improvements were made in the thermal and electrical characteristics of these joint blocks by the addition of thermal linkages and extra Nb_3Sn tapes between the blocks and the 4 K pothead dewars.

Unfortunately, the many thermal cyclings associated with these joint changes produced low temperature leaks in the conductor-helium flow system. These leaks appeared only below about 75 K but were of sufficient magnitude to degrade the test bed vacuum and preclude any effective temperature control in the helium flow system. Rework of several joints and seals where such leaks seemed most likely resulted in no improvement in the low-temperature behavior. Consequently, this sample and its container were removed from the test bed, possibly to be completely reworked and reinstalled at some future time.

III-2. Tests on Nb_3Sn Tape

We have obtained a Nb_3Sn tape, 1.27-cm wide with a 0.002-cm thick copper layer on each side of a Nb_3Sn-Nb-Nb_3Sn sandwich (IGC-9253). A description of the soldering of this tape to a 1.27-cm by 0.317-cm by 20-m copper substrate was described in Sec. V-2 of PR-9. As received, the tape appeared to be well bonded to the copper substrate except for a few irregularities around the 37.3-cm-diam hairpin bend at the conductor midpoint.

A 100-Ω heater was wound over a 5-cm length of the conductor approximately 2.5 m from the He exit port. Voltage probes were located at positions ± 0.03, ± 1.0, and ± 2.0 m from the heater midpoint in order to measure the thermally induced normal-superconducting interface propagation velocity by monitoring the times at which the normal zone (evidenced by the appearance of voltage change) arrived at the various probe positions. The sample tape was joined to each pothead lead by a set of bolted plates shunted by a 5-cm-wide Nb_3Sn superconducting tape.

Temperatures at six positions in the helium flow loop and at both joints, voltages at several positions along the sample, and current and time were monitored sequentially with the aid of a HP 3050A automatic data acquisition system. In addition, selected voltage pairs were monitored continuously on strip chart and X-Y recorders. The HP 3050A accumulated a set of eleven readings in approximately six seconds. For the first time, it was possible to determine what section of the conductor went normal first. Measurements of the critical current as a function of temperature are given in Fig. 11.,,. Several different experiments are represented, using both the battery-operated current supply and the three-phase rectifier supply. The relatively small scatter in the data indicates the relative precision of the current measurements on both power supplies. More importantly, the relatively large amount of ac ripple innerent in the rectifier supply had little or no effect on the $I_c(T)$ data., This is in agreement with the observation that no unusual voltage changes could be detected across the entire sample at currents less than $I_c(T)$ when using the rectifier supply. No temperature changes ascribable to ripple losses were observed.

For the majority of the data points, the thermometry information indicated that, as expected, $I_c(T)$ was first reached in the portion of the line nearest the helium exit from the flow tube, the warmest section of the conductor. However, I_c measurements near 12 K showed heating appeared near the middle of the loop. I_c degradation caused by the observed irregularities in the ribbon near the hairpin bend may be more important at some temperatures (or temperature gradients) than at others.

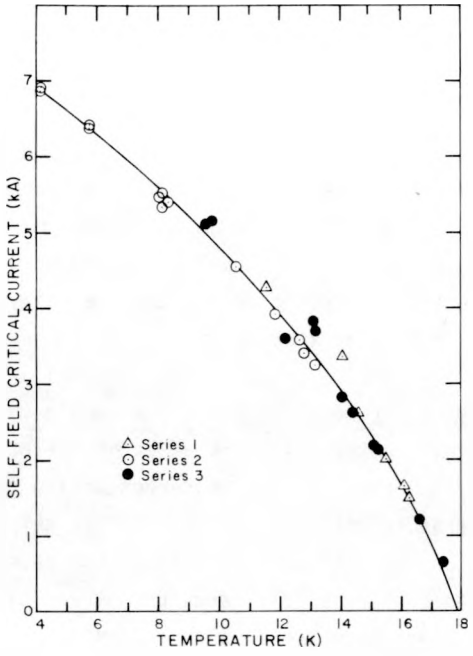

Fig. 11. Critical current vs temperature for a 20-m length of 1.27-cm-wide Nb_3Sn ribbon mounted on a copper substrate. The temperatures shown were obtained from the resistance thermometer mounted nearest the helium exit portion of the flow tube. This particular thermometer has not been calibrated, and the temperatures shown appear to be somewhat higher than expected.

In the earlier runs, the thermometers located at the joints proved the current was joint limited, whereupon the additional 5-cm-wide Nb_3Sn ribbons were employed to shunt the joints. Subsequent data have indicated stability in the joint areas. The data point at 4.0 K agrees reasonably well with the short sample critical current measurements for the same material, substantiating the conclusion that in the improved apparatus the current was not "joint limited", i.e., that the measured critical currents were a characteristic of the sample and were not influenced by the properties of the joints.

Figure 11 indicates a value of T_c (I=0), obtained by a small extrapolation, to be about 17.8 K. This is about 0.4 K higher than the value obtained in the short sample tests. Because of the isothermal nature of the short sample tests in liquid H_2, it is likely that T_c = 17.4 K is more nearly correct. It is possible that a small temperature difference exists between the sample at any point in the test bed and the resistance thermometer in the vapor at that point. Efforts to check this point and make necessary adjustments are underway.

Several data points, which exhibited I^2R heating and consequent temperature excursions at the joints, have not been included in Fig. 11. Improvements in the joints were made before starting a new series of experiments. The high data points in Fig. 11 probably result from the difficulty in observing the first appearance of a voltage due to the onset of dissipation because the normal resistance of the sample (tape + substrate) is only 3.5×10^{-6} Ω/m. Therefore the observed potential drop over the 20-m sample at the low currents is always small. So, under high current ramp rate and slow N-S zone propagation rate conditions, it seems possible to record high $I_c(T)$ values. Improvements in the sensitivity and noise of the X-Y recorder effectively eliminated this problem for most of the points designated as Series 2 and 3 on the graph.

Attempts were made to study the N-S propagation induced by a thermal pulse imposed while the conductor was carrying near-critical current. There was so much stabilization afforded by the heavy copper substrate that we could not initiate a propagating normal zone. A longer, more powerful heater will be incorporated in the next sample assembly.

IV. TRANSMISSION LINE DESIGN STUDIES

IV-1. Cryogenic Engineering

IV-1.1 Refrigeration

During this past quarter, purchasing arrangements were completed for a cryogenic refrigerator (CTI Model 1400) to provide cooling first for the 20-m test bed and later also for the Cable Engineering Test Facility. Additional instrumentation (carbon resistor temperature sensors) is being provided by LASL for installation by CTI. Calibration of four sensors was completed, and the sensors have been shipped to CTI. Plans have been made for the installation of the cold box by modification of an equipment room (Room 107 in SM-32, the cryo-engineering building) adjacent to the 20-m facility. These plans also include modification of a room to house the compressors and the moving of some equipment out of Room 107 to allow it to accommodate the Model 1400 refrigerator. Delivery of the refrigerator is now expected in September.

IV-1.2 Cable Engineering Test Facility

A Cable Engineering Test Facility (CETF) is in the planning stages. This facility will allow the testing necessary to complete a dc SPTL design as well as the testing of prototype portions of this design. During this past quarter an overall plan was made for development of this facility in several phases. The first phase will allow testing to begin on short sections (less than 3 m) in Room 109 of SM-32. Subsequent phases will provide the addition of high-voltage tests (up to 100 kV), extension of test section lengths to use both Rooms 109 and 111, and then lengthening the test sections to extend through the east wall of SM-32 and across the parking lot and unused land to the east of SM-32. Exact lengths of tests can not be given at this time because these lengths will be determined by the requirements of the individual tests and will be determined in the detailed test planning. However, lengths greater than 100 m may be anticipated for some tests. The final phase will incorporate testing to 450 kV.

IV-2. Cryogenic Enclosure Design

Computer codes have been developed for calculation of flow and pressure drop for supercritical gaseous helium in tubes. During this quarter we have begun code modifications to allow calculation of pressure drop in irregular cross sections.

In the previous progress report, cost equations for refrigerators and enclosures were developed. Three candidate designs for high-current, low-voltage applications were presented along with a list of design parameters that affect the cost. These parameters have been analyzed to allow a reduction in their spread. Appropriate values have been chosen and the capital cost of the cryogenic system for these three designs plus two additional designs (discussed below) have been evaluated. The fifth design is for a high-voltage, low-current application compatible with conventional dc transmission equipment.

IV-2.1 Design IV

A design for a flexible low-voltage, high-current cable using wrapped dielectric tapes is shown in Fig. 12. The go helium is in the central cooling channel of the cable at a pressure of 10 to 15 atm. The helium is expanded and returned in the space between the cable and the enclosure inside wall at a pressure between 3 and 5 atm. As in Design III, thermal contact exists between the go and return streams. The cable is a coaxial monopole with a grounded shield.

IV-2.2 Design V

A design for a flexible, high-voltage, low-current cable using wrapped tapes is shown in Fig. 13.

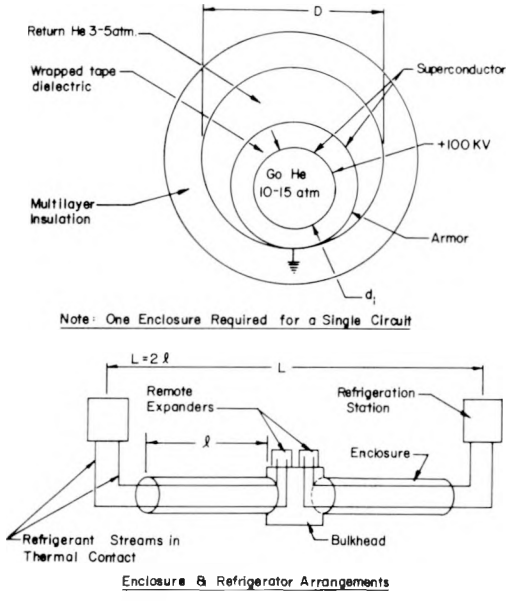

Fig. 12. Cryogenic enclosure of Design IV.

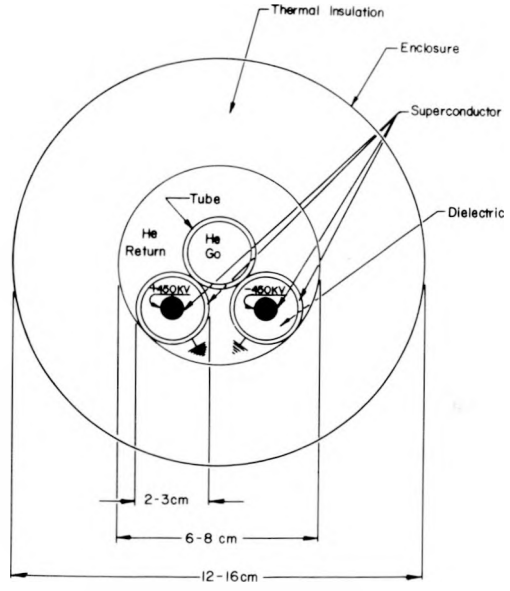

Fig. 13. Design V for bipolar operation with high voltages and electrical stresses.

Wrapped tapes surround each of the three conductors and another conductor is wrapped on each surface. The inner conductors operate at ± 450 kV in a balanced bipolar mode. The outer grounded conductors normally carry the unbalanced current. In the event of a fault on one pole, the outer conductor of the other pole can carry the return current allowing operation at half power to continue.

A separate tube carries the go helium at 10 to 15 atm pressure to remote expanders where it is expanded to 3 to 5 atm and returns in the space between the cables and the enclosure inside diameter. Thermal contact exists between the go and return streams.

IV-2.3 Parameter Analysis

IV-2.3.1 Enclosure Thermal Performance

The most important parameter from the viewpoint of cryogenic system cost has been found to be the enclosure thermal performance. A large heat influx through the thermal insulation results in a large flow rate requirement and a corresponding large cooling channel diameter and enclosure cost. In order to reduce the heat influx, a low value of apparent thermal conductivity in the insulation is required.

Many measurements of apparent thermal conductivity of multilayer insulation have been made in the laboratory, and values of about 0.25×10^{-4} W/m-K are commonly obtained. When the insulation is applied to a pipe with spacers separating the pipe from an outer vacuum jacket, the apparent thermal conductivity is generally greater than these values. The measurement of the thermal influx into a Kabelmetal enclosure at BNL[1] allows the calculation of a commercially available thermal insulation performance. An apparent thermal conductivity of 3.5×10^{-4} W/m-K was obtained. However, we expect that from an insulation development program the apparent thermal conductivity might be reduced to 1 to 2×10^{-4} W/m-K.

The enclosure diameters and thermal influx are related to each other by the equation of the apparent thermal conductivity, which for concentric cylinders has been solved for the diameter ratio between the outside and inside of the enclosure. The resulting equation is:

$$D_o/D_i = \exp \frac{2\pi K \Delta T}{\dot{Q}/L} , \qquad \text{(IV-1)}$$

where K = apparent thermal conductivity, ΔT = temperature difference across the insulation, $\dot{Q}$ = total thermal influx, and L = length.

It is convenient to define the thermal performance of the enclosure by the term $\dot{Q}/L$ in W/m. Equation (IV-1) has been evaluated for several values of thermal performance with results given in Fig. 14. It is desirable to keep the diameter ratio to 2 or less. If apparent thermal conductivity of 1 to 2×10^{-4} W/m-K is obtained, a thermal performance of 0.25 to 0.5 W/m can be obtained.

Refrigerated radiation shields may be used to intercept the thermal influx, with a resultant trade of some 10-13 K refrigerator capacity for refrigerator capacity near 100 K. The 10-13 K coolant channel diameter may thereby be reduced, but the enclosure diameter must be somewhat increased to carry the refrigerant pipes for the shield refrigeration. The refrigerated shield makes the cryogenic system more complex, increasing the capital and installation cost. The refrigeration cost saved at 10-13 K tends to be compensated by the cost of the shields and the cost of 100 K refrigeration. The size of the enclosure remains nearly the same for shielded or unshielded designs. Detailed calculations of these effects suggest that no clear economic advantage is gained by using a refrigerated shielded system. From the viewpoint of installation cost and system reliability, it is highly desirable to avoid the refrigerated radiation shielded design.

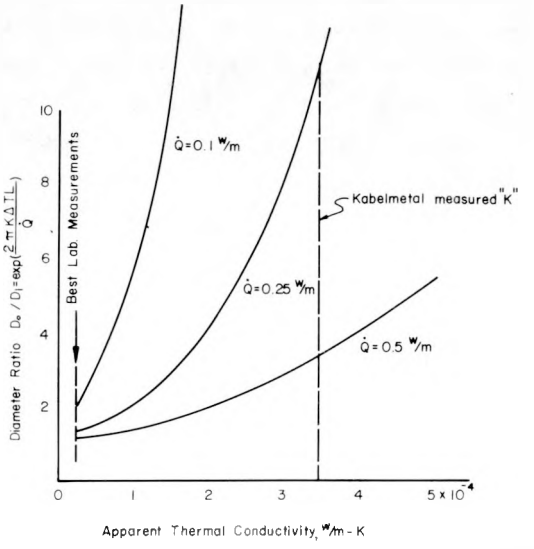

Fig. 14. Diameter ratio as a function of insulation and thermal performance of enclosures without refrigerated shields.

IV-2.3.2 Friction Factor

In the previous progress report the diameter of the cooling channel was shown to be directly proportional to the friction factor to the 1/5 power. The friction factor may be calculated from:

$$f = 0.046 \left(\frac{\dot{m}}{b\mu}\right)^{-0.2} n \ , \qquad \text{(IV-2)}$$

where $\dot{m}$ = mass flow rate, b = wetted perimeter of cooling channel, μ = viscosity of helium, and n = roughness multiplier, which must be experimentally determined. Again from BNL experimental helium flow data[2], n = 7 for corrugated tubes. If a smooth tube design requires a 10-cm-diam cooling channel, a corrugated tube design will require a 15-cm-diam cooling channel. According to the cost equation for enclosures, the corrugated design will cost about \$0.1 x 10^6/mile more than the smooth tube design.

It is essential to use either smooth cooling channels or a smooth liner where corrugated cooling channels must be used. However, several designs require that cables of unknown roughness lie in the bottom of a cooling channel. The required cooling channel diameter will eventually have to be established by full scale experiments on long test sections.

IV-2.3.3 Allowable Pressure Loss

A compressor-powered circulation system can be made to operate with a refrigerator system power increase of about 10% per atm of pressure loss in the load. A 5-kW refrigerator with no pressure loss costs about \$0.77 x 10^6. A one-atm pressure loss in the load will increase the cost to \$0.82 x 10^6, or by 6.5%.

A multistage centrifugal pump might develop a one atm pressure rise. The increase in the refrigerator power needed to absorb the pump work is given by:

$$B = \frac{\Delta P}{\eta \rho C_p \Delta T} \ , \qquad \text{(IV-3)}$$

where ΔP = pressure loss, η = pump efficiency, ρ = helium density, C_p = specific heat of helium, and ΔT = temperature rise at the load.

Evaluating Eq. (IV-3) for ΔT = 2 K, C_p = 6.5 kJ/(kg • K), ρ = 50 kg/m^3 (likely design condition for LASL), and a pump efficiency of 50% gives a refrigerator power increase of 41%. The 5-kW refrigerator cost increases to \$0.93 x 10^6, or by 21%. The designer must not arbitrarily double the pump loop operating pressure to increase the density and halve the power loss since this will increase the helium inventory. A reciprocating pump might be used to increase the pump efficiency, but then the system reliability will be reduced.

A one-half atm pressure-loss design may typically result in an enclosure diameter of 9 cm and an enclosure cost of \$0.45 x 10^6/mile. Increasing the pressure loss to 1.5 atm will reduce the diameter to 7 cm and the cost to \$0.4 x 10^6/mile. This results in a savings for Design I of \$10 x 10^6 over a transmission distance of 100 miles. Figure 15 shows the relationship between pressure loss and diameter for Design I. In order to achieve an enclosure cost saving (diameter reduction), the pressure loss should be at least 1 atm, but not much is gained by going over 2 atm because the pumping losses are excessive, making the refrigerator cost at least 15% greater (not including the pump cost) than that of a compressor-powered circulation system.

IV-2.3.4 Allowable Temperature Rise and Inlet Temperature

The effect of the temperature rise on the linear current density is seen in Fig. 16. An increase of the temperature rise reduces the obtainable stable current density and reduces the inlet temperature while increasing the refrigerator cost. With the outlet temperature limited to 13 K, if the temperature rise is allowed to increase more

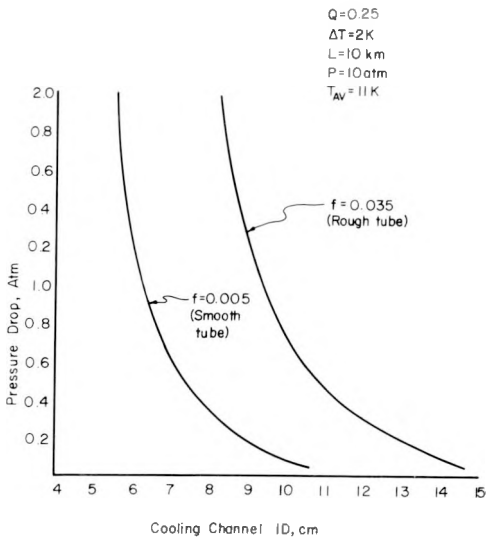

Fig. 15. Pressure loss in a circular passage, Design I.

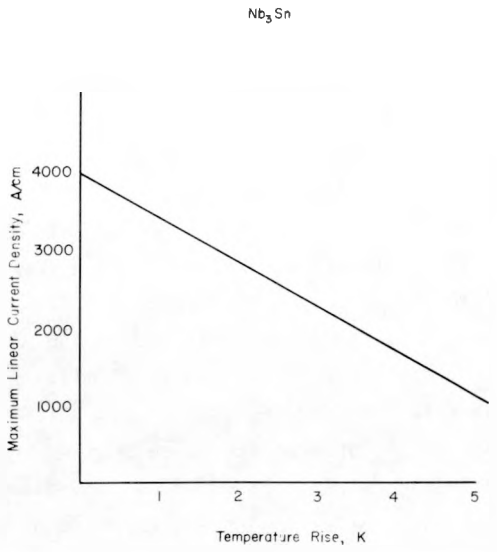

Fig. 16. Effect of the allowable temperature gradient along the conductor on the adiabatic stable linear current density.

than 3 K, the refrigerator power is charged at a temperature less than 10 K and the obtainable stable linear current density drops to below 2000 A/cm. In the high-current, low-voltage Designs I through IV, it is desired to keep the linear current density above at least 2000 A/cm.

The enclosure diameter can be reduced 15% when the temperature rise is increased from 2 to 3 K. This will result in a cost savings of about $\$1.5 \times 10^6$ in Design I over a distance of 100 miles; thus a 3 K temperature rise is indicated.

The above temperature rise discussion is limited to Designs I and II. The other designs with thermal contact between the go and return streams are special cases requiring expanders where the temperature decreases with distance from the refrigerator. The rate of temperature reduction depends on such factors as the operating pressures, the heat transfer, and the expander efficiency.

IV-2.3.5 Refrigeration Ratio

When the inlet temperature is fixed at 10 K and the outlet temperature is 13 K, the log mean temperature is 11.4 K. Applying the Carnot principle between 300 and 11.4 K results in a theoretical refrigeration ratio of 25.2. The refrigeration ratio is defined as the ratio of refrigerator room temperature input power in watts to low temperature refrigeration, also in watts. Refrigeration efficiency is defined as % of the theoretical or Carnot refrigeration ratio. For this case a refrigeration ratio of 150 implies a refrigeration efficiency of 17%. As 17% is readily obtainable, a refrigeration ratio of 150 will be used in our design considerations.

IV-2.3.6 Refrigerator Redundancy

A redundancy of two has been chosen to increase the reliability. Each refrigerator station will have two refrigerators.

IV-2.3.7 Power Levels

The designs we are considering are for cables with from 2-to 5-GW capacity. The inner diameter of the coolant channels of Designs III and IV is given as 5 cm, or a circumference of 15.7 cm. This circumference, if plated with a superconductor with a linear current density of 2500 A/cm, could carry 39.3 kA. Applying 100 kV to this current results in 3.9 GW of power.

Design V requires only 5 500 A to provide 5 GW.

IV-2.3.8 Summary of Parameters

Parameters chosen to reduce the cryogenic systems cost are:

Enclosure thermal performance - $\dot{Q}/L = 0.25$ W/m
Friction factor - according to Eq. IV-2
Refrigerator redundancy - 2
Allowable pressure loss - 1 atm
Temperature rise - 3 K
Inlet temperature - 13 K
Refrigeration ratio - 150 with no pressure loss.

The refrigerator spacing has been left as a variable. Costs of the candidate designs will be calculated as a function of refrigerator spacing.

IV-3. Cost Estimates

IV-3.1 Cryogenic System Capital Cost of Design I

Cooling channel diameters for Design I have been calculated in accordance with Eq. (IV-2) for several refrigerator spacings and the parameters listed in Sec. IV-2.3.8. These diameters, shown in Fig. 17, have been used to calculate the cost of the enclosures and refrigerators as indicated in the previous report.

Figure 18 shows the effect on cost of varying the refrigerator spacing and pressure loss for Design I. The refrigerator power ratio has been increased at a rate of 10% per atm for the corresponding pressure losses. The choice of 1 atm as a design pressure loss is confirmed. Also see Fig. 15.

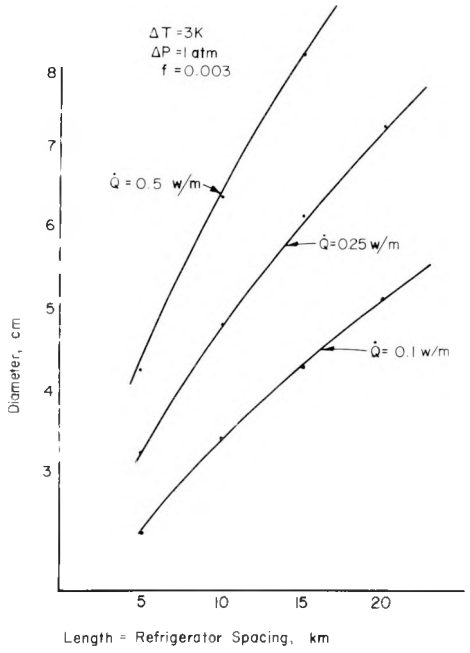

Fig. 17. Diameter of Design I cooling channel as a function of refrigerator spacing for several cryogenic enclosure thermal performance values.

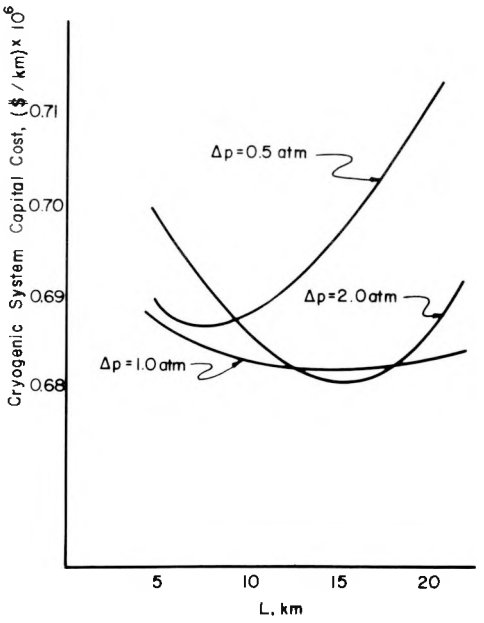

Fig. 18. Capital cost as a function of refrigerator spacing and pressure loss for Design I.

IV-3.2 Cryogenic System Capital Cost of Design II

The diameter of the cooling channels for Design II must be larger than those of Design I in order to compensate for the pressure loss caused by the increased surface area of the annular passage and the flow around the dielectric spacer. The space requirement for flow in an annular passage is found from:

$$(D_o^2 - D_i^2)^2 \quad (D_o + D_i) = \frac{32\ \dot{fm}^2 L}{\pi^2 \Delta P\ \rho} . \qquad \text{(IV-4)}$$

An additional allowance must be somewhat arbitrarily made for the spacers, as at this time the number and size of these spacers is not known. Estimated diameters are given in Fig. 19. Costs based on these diameters are given in Fig. 23.

IV-3.3 Cryogenic System Capital Cost of Design III

The annular space requirement for the helium flow is calculated from Eq. (IV-4). However, the diameter of the inner helium channel must first be calculated from the usual pressure-loss equation.

The mass flow rate for this design with thermal contact between the go and return streams is calculated from an energy balance around the lower end of the refrigerator, including the enclosure, and is:

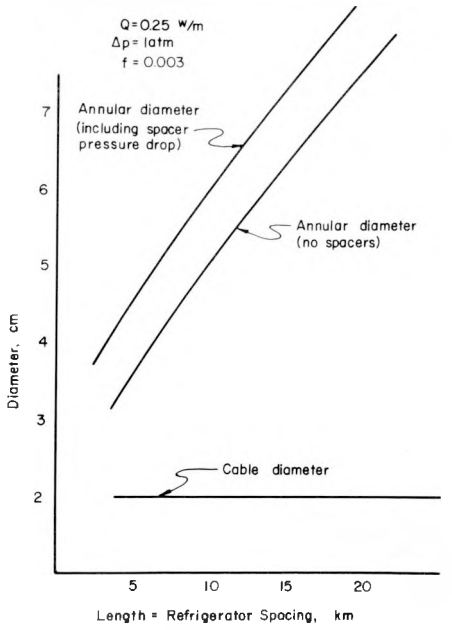

Fig. 19. Diameters of Design II cooling channel as a function of refrigerator spacing.

$$\dot{m} = \frac{(\dot{Q}/L)\, L}{\Delta h_{enc.} + \Delta h_{exp.}} \qquad \text{(IV-5)}$$

where $\Delta h_{enc.}$ = enthalpy difference at the warm end of the enclosure and $\Delta h_{exp.}$ = enthalpy difference across the expander.

The approximate values used in these calculations are $\Delta h_{enc.}$ = 11 J/g and $\Delta h_{exp.}$ = 5 J/g. The true values will depend on the heat exchanger and expander efficiencies.

Equations (IV-4) and (IV-5) have been evaluated as a function of length for a go stream pressure of 10 atm and a return stream pressure of 3 atm. Again an allowance for spacers has been made. The resulting diameters are given in Fig. 20.

Since the return helium acts as the dielectric, the electrical stress must be calculated and may be obtained from:

$$S = \frac{E}{D_i \ln (D_o/D_i)} , \qquad \text{(IV-6)}$$

where E = the applied voltage.

In the low-voltage design of E = 100 kV the electrical stress is always less than 5 MV/m. This low value presents no problem.

The cost of this design has been calculated and is presented in Fig. 23.

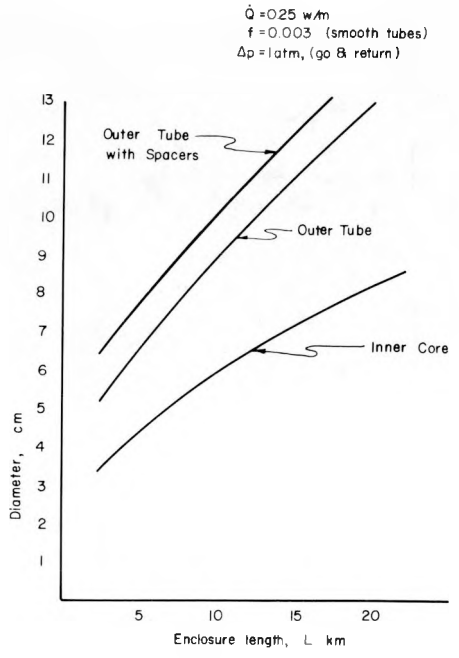

Fig. 20. Diameters for Design III as a function of enclosure length.

IV-3.4 Cryogenic System Capital Cost of Design IV

The inner diameter of the cable cooling channel is the same as the inner diameter of Design III. The outer diameter of the cable is set by the electrical stress requirements of the dielectric. The thickness of the dielectric tapes is calculated from:

$$t = \frac{D_i}{2} \exp\left(\frac{E}{S_a D_i} - L\right) , \qquad \text{(IV-7)}$$

where S_a = allowable electrical stress. The thickness has been calculated using E = 100 kV and S_a = 10 MV/m.

The space required for the return helium flow is calculated from Eq. (IV-4). The cable outside diameter is the D_i of Eq. (IV-4). Space requirements are shown in Fig. 21. Costs for Design IV are plotted on Fig. 23.

IV-3.5 Cryogenic System Capital Cost of Design V

The thickness of the wrapped tapes is calculated from Eq. (IV-7). According to the data compiled in NBS Monograph 132 the breakdown voltage of selected paper and polymer tapes exceeds 100 MV/m in a cold helium environment. A design stress of 60 MV/m has been used to establish the cable insulation thickness requirement of 0.9 cm. The resulting cable diameter is 3 cm.

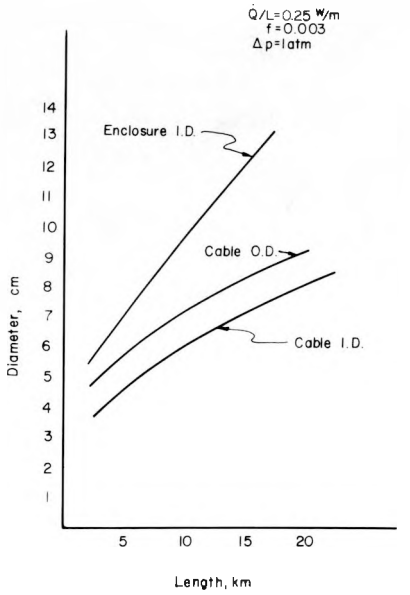

Fig. 21. Diameters required for Design IV as a function of enclosure length.

The enclosure inside diameter has been calculated in accordance with the general form of the pressure loss equation:

$$\frac{A}{b} = \frac{f\dot{m}^2 L}{2\Delta P \rho}, \qquad \text{(IV-8)}$$

where A = cross-sectional flow area of enclosure with the cables in place and b = wetted perimeter.

The tube enclosure diameters required have been established by Eq. (IV-8) and are shown in Fig. 22. Costs have been calculated and are shown in Fig. 23.

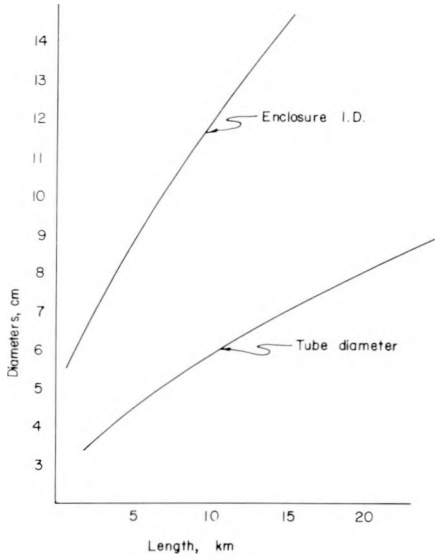

Fig. 22. Diameters required for Design V.

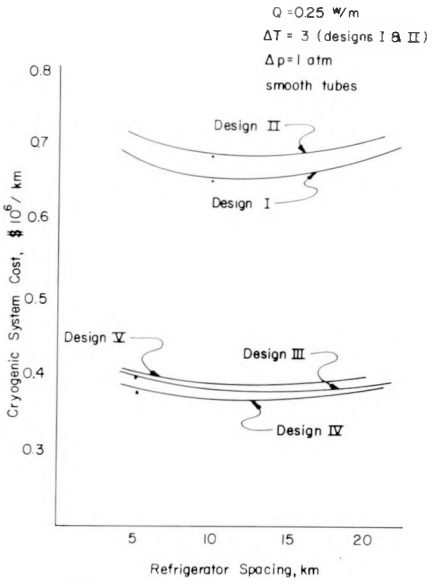

Fig. 23. Comparison of cryogenic system cost for five designs as a function of refrigerator spacing.

IV-4. Cost Estimates

The dimensions and parameters developed in this reporting period have been applied to the cost equations of the previous report. The results plotted in Fig. 23 represent the expected minimum capital cost of the cryogenic system. Rougher tubes and higher thermal influxes will drive the cost up.

Refrigerator spacing is not a problem as the cost is a weak function of this distance. At short distances more of the cost is in the refrigerators, while at longer distances the enclosure is the major expense.

The use of thermal contact between the go and return streams (Designs III through V) gives a large cost reduction over those designs that require separate enclosures (Designs I and II) for the refrigerant streams.

There is no outstanding choice between Designs III, IV, and V when only cost is considered according to Fig. 23. However, the choice becomes clearer when total cost is compared with competing systems. The BNL cost analysis has shown that the cryogenic system capital cost is about 50% of the total cost for an ac superconducting system.[3] The enclosure size of a dc superconducting system will be smaller than for an ac system and thus will have a lower installation cost. On the other hand, the BNL trenching cost estimate was based on Long Island conditions that produced low values. Trenching cost can normally be expected to be higher. Thus a rough estimate of the total cost may be made by multiplying the figure of 0.4×10^6/km from Fig. 23 by two to give an installed cost estimate of 0.8×10^6/km.

Figure 24 shows the cost on a per MVA-mile basis. Terminal cost has been estimated at $32/kW. The cost including the terminals are shown with solid lines while the cost without terminals are shown as dashed lines. Power levels of 1 GW will not allow the dc superconducting system to compete economically with conventional underground power transmission systems, even without considering the terminals. The dc superconducting system becomes competitive with ac superconducting systems at distances greater than 160 km and at power levels of 5 GW and larger.

The only way for a dc superconducting system to be competitive at short distances is to become

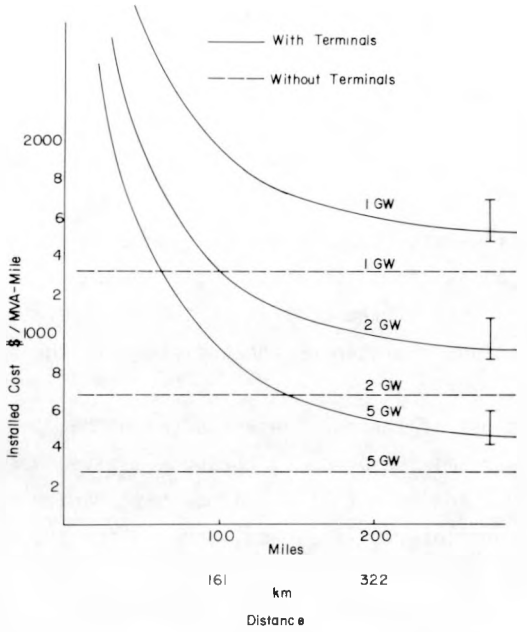

Fig. 24. Installed cost estimates of dc superconducting systems.

an extension to a 2-GW or greater overhead dc line. Thus, the terminal costs need not be charged to the underground dc superconducting system. This means that high voltages might be necessary.

IV-5.. References

1. J. Dean and J. Jensen, "Supercritical Helium Refrigerator for Superconducting Power Transmission Cable Studies," Cryogenic Engineering Conference, Paper R7, Kingston, Ontario, Canada, (1975).
2. J. Dean , private communication with A. Mead, Brookhaven National Laboratory, Cold Neutron Moderator Project (1975).
3. E. Forsyth , G. Mulligan, J. Beck, J. Williams, "Technical and Economic Feasibility of Superconducting Power Transmission, A Case Study," Paper T74462-8, IEEE Summer Meeting (1974).

V. SUPERCONDUCTING MATERIALS DEVELOPMENT

V-1. Introduction

Superconducting materials development and fabrication methods have been concentrated in the following areas: 1) a two-sided Nb_3Sn conductor for the 20-m test bed is being fabricated; 2) several short sample test specimens have been fabricated from multifilamentary Nb_3Sn wires; 3) a study of mechanical damage in Nb_3Sn tapes has been started using acoustical emission techniques in conjunction with tensile tests; 4) grinding experiments aimed at making superfine Nb_3Sn powder are underway; 5) sputtering investigations have been continued and coatings are being made at high deposition rates; 6) the work on Nb_3Ge by CVD has been continued with the emphasis on controlling the oxygen content; and 7) an apparatus has been constructed to CVD coat the exterior of a copper tube to make superconducting pipes up to 900 mm long.

V-2. Nb_3Sn

V-2.1 Fabrication of a Two-Sided Test-Bed Conductor

A superconducting specimen is being prepared for the 20-m dc SPTL test bed by soldering superconducting Nb_3Sn tapes to both sides of a hairpin-shaped copper strip 3.2 mm thick by 12.7 mm wide by 20 m long. The basic technique used for this type of soldering operation was developed for the single-sided conductor made earlier for the test bed (PR-9). The single-sided tape was soldered to the substrate on the straight lengths using a soldering fixture made for that purpose, but the bend area was soldered manually.

An entirely new soldering apparatus was constructed to solder the two tapes to the substrate simultaneously, as well as to track around the bend. After several modifications to improve tracking and heating properties, it is ready to use.

V-2.2 Short Sample Fabrication

Several special short sample specimens have been prepared from the Harwell unreacted multifilamentary Nb_3Sn wire mentioned in PR-8, Sec. II-1.4. These specimens were about 25 cm long and included the following geometries: 1) a three-strand Nb_3Sn twisted cable; 2) a six-strand Nb_3Sn cable wrapped over a solid copper core; and 3) a six-strand Nb_3Sn cable wrapped over a stranded copper core. Each Harwell Nb_3Sn wire contained 3145 filaments. After the cables were formed they were heat treated at 750°C for 60 h to form the Nb_3Sn filaments and bonded together using lead-tin solder.

V-2.3 Mechanical Damage in Nb_3Sn Superconducting Tapes

The Nb_3Sn in composite superconducting tapes is formed in very thin, very brittle layers. Any damage to these layers could cause a degradation of the current-carrying capacity of the tape. Photomicrographs of unstressed Nb_3Sn tapes are shown in Fig. 25. The outer layers are copper, thinly coated

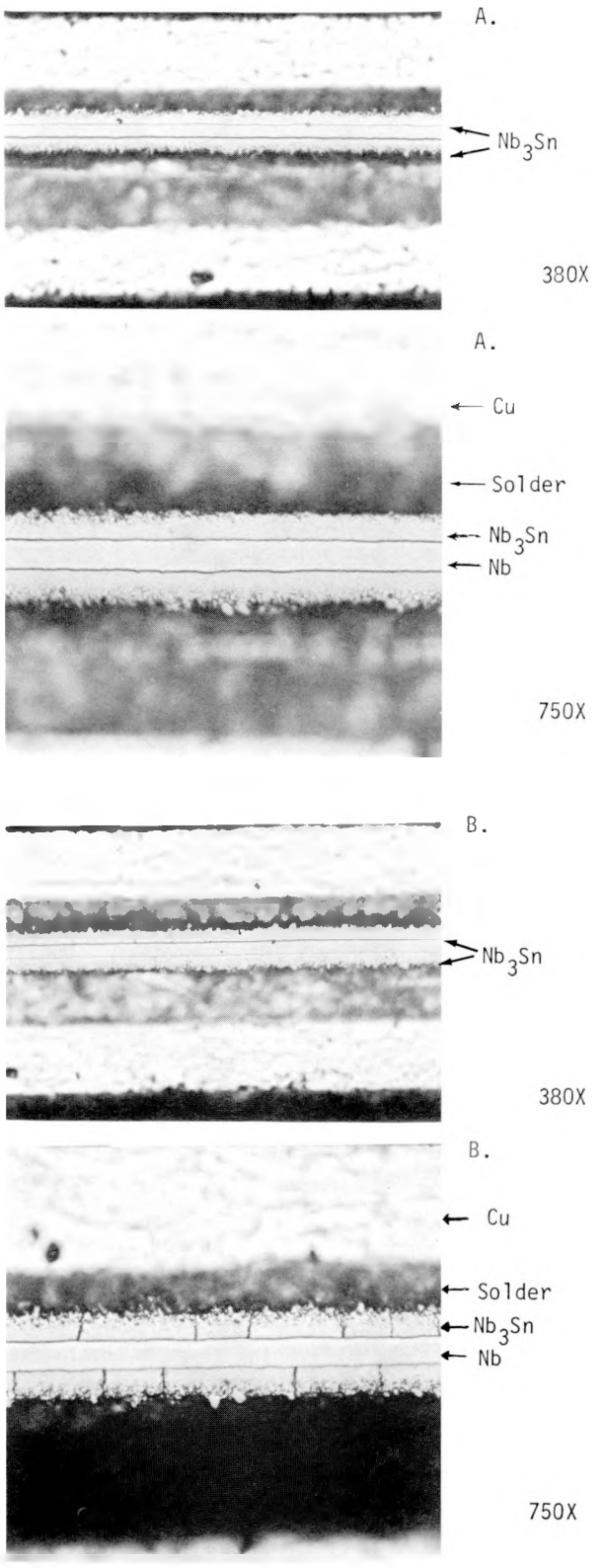

Fig. 25. Photomicrographs of the cross section of Nb_3Sn tapes at two magnifications: A) unstressed sample; B) stressed sample. Note cracks in the Nb_3Sn layers.

with lead-tin solder. The layer just inside the copper is lead-tin solder which bonds the superconducting materials to the copper. The central core is Nb with surface layers of the superconducting and brittle Nb_3Sn.

It would be useful to know the tensile strength and strain at which the intermetallic compound first starts to fracture. Acoustical emission looks promising as a method for the detection of fracture during normal handling operations involving tapes. This method involves stressing a specimen while "listening" to the output of a small acoustical transducer mounted on the specimen. The transducer output is normally displayed on an oscilloscope or data recorder, but it can be also monitored audibly. Acoustical emission can be a sensitive tool and, by coupling it with other tests, the effects of stress on tape properties can be studied.

Tensile specimens of Nb_3Sn tapes were prepared by soldering a 1.25-mm-thick copper sheet on both sides of a 20-cm-long tape. The middle third of the tape was not altered. The thicker end-regions cushioned the bearing stresses of the tensile grip. Any noise due to grip slippage or damage to the tape by the grips must be avoided.

After preliminary checks with Cu and Nb, several Nb_3Sn tape specimens were tested and good acoustical and stress-strain data obtained. Figure 26 shows a typical stress-strain curve for the Nb_3Sn

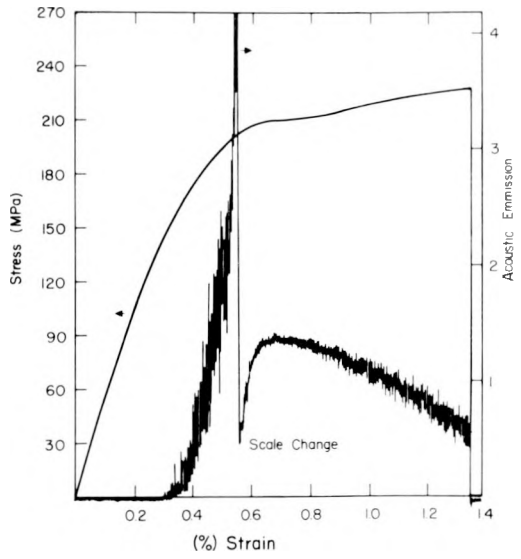

Fig. 26. Superconducting tape tensile test curve and acoustic emission.

tapes with the simultaneous acoustical emission trace superimposed. The acoustical emission ordinate is in arbitrary units; a 10X scale factor reduction occurs at about 0.6% strain.

Test results on three Nb_3Sn specimens are shown in Table I. These values are in reasonable agreement with each other considering the brittleness of the material.

TABLE I
STRESS AND STRAIN VALUES FOR THE FIRST FRACTURE NOISE ON Nb_3Sn TAPES

Test No.	First Fracture Indication	
	Stress (MPa)	Strain (%)
1	99	0.2
2	101	0.22
3	147	0.3

A metallographic examination of the tapes was made and the photomicrographs are shown in Fig. 25B. The specimens were cathodically etched longitudinal sections. The top pictures, A-1 and A-2, were taken prior to testing and the bottom ones after the composite tape had been tested to failure. No cracks are apparent in the top pictures, but severe cracking in the Nb_3Sn layer has occurred during testing as shown in Figs. B-1 and B-2. The cracks stop abruptly at both the solder-Nb_3Sn and Nb-Nb_3Sn interfaces. Presumably these cracks extend completely across the tape and would have caused catastrophic failure of the superconductor.

The feasibility of using acoustic emission combined with tensile testing to detect first fracturing of the superconducting Nb_3Sn layer has thus been demonstrated. An indication that the stress and strain needed to cause this initial fracturing will vary has been observed; however, a more sensitive method, such as J_c measurements, is needed to assess the damage done by the first fracturing. Eventually similar experiments at cryogenic conditions will be performed.

V-2.4. Fine Powder Production Experiment

Several preliminary experiments aimed at making very fine powders of superconductors by commutation processes were encouraging, although a considerable amount of contamination was encountered. To reduce this contamination a niobium-lined ball mill was constructed and used in an argon atmosphere box with tungsten rods to grind Nb_3Sn powder.

Samples of the Nb_3Sn powder were ball milled for various lengths of time — 1, 4, and 7 days. The superconducting properties of these samples showed very little change after ball milling up to 4 days, as shown in Table II. Particle sizes will be determined by an adsorption technique.

TABLE II
SUPERCONDUCTING PROPERTIES OF BALL MILLED Nb_3Sn POWDER

Time of Commutation (h)	T_c (K)	ΔT_c (K)	Relative Signal Strength
24	18.1	1.5	5.0
96	17.9	2.0	6.8
264	17.9	2.0	3.2

V-2.5 Sputtering

Sputtering is a common method of producing superconducting films on various substrates, and with the rather widespread availability of high-rate sputtering apparatus it becomes potentially useful for making conductors.

An rf power source for our Sloan Sputtering Gun apparatus has been put into operation. Coating rates of over 1500 Å/min are routine. Using a cathode of $Nb_3(Al,Ge)$ produced by the cold press-sinter process, strongly-adherent, mirror-like, amorphous films were obtained. Thermal cycling between room temperature and 4 K produced no visible effects.

A substrate heater has been constructed for the system and at present a substrate temperature of about 775 K can be obtained. A number of materials have been deposited on heated substrates with excellent bonds. Additional sputtering experiments are planned with emphasis being to form the A-15 compound directly.

V-3. Basic Studies of the Nb_3Ge Chemical Vapor Deposition Process

V-3.1. General

In the Nb_3Ge program efforts have been directed toward producing a more uniform and homogeneous coating by the CVD process. The exact composition of the coating is being investigated. Since the material showing the highest T_c values is not single phase (10-20% of a second phase is

present), it is not possible by means of chemical or other bulk analyses to determine precisely the composition of the A-15 phase. The second phase was originally assumed to be Nb_5Ge_3, but this assumption has not been fully substantiated. Our inability to determine the exact composition of the A-15 phase has prevented us from understanding the role oxygen plays in these materials and is causing great difficulty in the long-range ordering experiments being pursued by Sweedler and Cox[1] at BNL. Therefore, a necessary first step in improving Nb_3Ge is the production of a single phase by exercising better control over the composition of the gas stream, particularly the amount of $NbOCl_3$, and by eliminating gravity or convection effects in the coating chamber.

V-3.2 Oxygen Content

As indicated in PR-9, high T_c stoichiometric material seems to have the sharpest x-ray structure when it contains approximately 4 – 4.5 at.% oxygen. Current density measurements (Sec. II-1) seem to indicate that the highest current densities also occurred in the region of 4 at.% oxygen. This conclusion, based on the measurement of only 5 specimens plus an additional measurement published by Gavaler et al.[2] on material prepared at Westinghouse Laboratories, must be interpreted cautiously until more samples can be measured. It is clear, however, that it is important to be able to put in a predetermined and uniform amount of oxygen.

The most practicable form in which oxygen can be made available is $NbOCl_3$, either added as such or generated during the process. Initial attempts to generate $NbOCl_3$ have consisted of adding an Ar-1% O_2 mixture to the hydrogen prior to the preheater. The intent was to form water vapor in the preheater, which in turn would react with the $NbCl_5$ to produce $NbOCl_3$. Tests of this system showed that even when an amount of oxygen was added sufficient to convert from 5-7 at.% of the $NbCl_5$ to $NbOCl_3$, only approximately 0.5 at.% O_2 was deposited in the coat. Further tests on the components indicate that the oxygen is reacting to form water vapor, but that the water vapor is being gettered in the hot vaporizer, probably by $NbCl_3$, before it has a chance to react with the $NbCl_5$ vapor. As an alternative, a new chamber is being installed so that either water vapor or oxygen may be added to this chamber to oxidize the $NbCl_5$ prior to the introduction of hydrogen.

V-3.3 Gravity or Convection Effects

Occasionally the appearance of the niobium-germanium deposits suggests that due to the large difference in densities of the coating gases, some stratification may occur in the horizontal deposition chamber being used. A vertical system has been assembled in which the coating gases pass from the top to the bottom of a 600-mm-long copper chamber, and initial tests with this reactor are very encouraging. The desired oxygen content has not yet been achieved (the first coats contain only about 0.1 wt% O_2), so it has not been possible to prepare high T_c homogeneous material; however, material slightly deficient in germanium and having T_c's from 16.8 – 18.5 K has been prepared with an unusually sharp x-ray pattern.

V-3.4 Niobium-Silicon System

Single phase Nb_3Si having an A-15 structure has been produced by the CVD process operating in the temperature range from 875°C to 975°C. Relatively sharp x-ray patterns with lattice spacings ranging from 5.21 – 5.135 Å were obtained. On the basis of the Geller[3] model prediction of 5.08 Å for stoichiometric Nb_3Si, the smallest lattice achieved, 5.135 Å, corresponds to ∿ 18.5 at.% Si. The T_c of this material, measured under applied fields ranging up to 5 T (to suppress the transition of the niobium undercoat) is ∿ 7.5 K, a number consistent with the estimated composition. Over the temperature range covered, the lattice spacing of the best material produced changed very little, implying that we may be in the region of a vertical phase boundary such as is found for Nb_3Ge at higher temperatures. This further implies by analogy that if a retrograde phase boundary extending to higher silicon content exists, it will occur at a lower temperature, perhaps as low as 400 – 600 °C. Investigation of this point is severly hampered by the stability of the silicon halides below 900°C.

V-3.5 Niobium-Germanium-Silicon Ternary System

Approximately ten samples have been made at 900°C on the germanium-rich side of the Nb_3Ge – Nb_3Si pseudobinary. As germanium is replaced by silicon, the temperature at which the stoichiometric A_3B is stable appears to be rapidly depressed.

Coats of composition up to $Nb_3(Ge_{.9}Si_{.1})$ can be prepared without any degradation of T_c. At the composition $Nb_3(Ge_{.82}Si_{.18})$, T_c is lowered to 19 — 19.5 K. This implies that in order to study the ternary system the deposition temperature needs to be decreased as the silicon content is increased, but reduction of the silicon halides becomes progressively harder.

Two observations of interest concerning the alloy $Nb_3(Ge_{.86}Si_{.14})$ are worth mentioning. The self-field current density of this composition was about 1.2×10^6 A/cm^2 at 13.8 K, a value comparable with the better oxygen-containing niobium-germanium samples. Metallographic examination indicated a rather dramatic difference in grain size, however. The niobium-germanium-silicon was composed almost entirely of submicron grains, while the niobium-germanium-oxygen material, as noted previously, is composed of grains in the range of 2-5 μm.

V-3.6 References

1. A. R. Sweedler and D. Cox, "Neutron Irradiation Effects in Superconducting A-15 Compounds," Presented at the Conference on Defect Property Relationships in Solids, Princeton University, March 24, 1975.
2. J. R. Gavaler, M. A. Janocko, A. I. Braginski, and G. W. Roland, IEEE Transactions on Magnetics MAG-11, 192 (1975).
3. G. R. Johnson and D. H. Douglass, J. Low Temp. Phys. 14, 565, (1974).

V-4. Continuous CVD of Niobium-Germanium on the Exterior of Copper Tubing

A CVD apparatus that coats the exterior of a 17.7-mm-o.d. copper pipe has been designed and constructed. The copper pipe that serves as the substrate simultaneously rotates and traverses through the coating chamber. Coating lengths of 890 mm have been obtained.

A gaseous mixture of hydrogen, argon, $GeCl_4$, and $NbCl_5$ is preheated and allowed to react on the hot surface of the pipe. The composition of the gaseous mixture, its temperature, the substrate temperature, the rotational speed and traversing speed of the pipe are among the variables that can be controlled during the coating process.

To date materials with various coating conditions have been tried resulting in T_c values of 15 to 17 K.

VI. OUTSIDE CONTRACTS

VI-1. LASL

Several outside contracts were placed during this quarter. Results from these contracts will be discussed in future progress reports.

A contract was placed with Intermagnetics General Corporation, Guilderland, NY, to furnish Nb_3Sn tapes manufactured under a wide variety of controlled conditions. A few of the parameters to be varied are reaction time and temperature, niobium and tin purity, Nb_3Sn thickness, and surface condition. I_c data at 4 K with transverse applied fields of 5 and 10 T will be furnished for each sample. Self-field critical currents, T_c, and possibly some ac loss measurements will be made at LASL to help determine whether a superior superconductor for dc SPTL application might be produced by the tin diffusion process and whether correlations useful in developing higher $T_c - J_c$ Nb_3Sn might be found.

A contract was awarded to Cryogenic Consultants Inc. to study several aspects of cryogenic enclosure design. This study (approximately 2 man-months) has been completed. It includes estimates of practically obtainable heat leaks, line costs, and an independent verification of our earlier pressure drop calculations.

A contract was awarded to Prof. E. Lady of the University of Michigan for further study of thermal contraction in special expansion bellows and pressure drops in expansion bellows and irregular cross sections. This work will be performed in FY 76.

The first phase of a contract for developing a mathematical model of a dc SPTL has been completed under a contract with the Electrical Power Engineering Department of New Mexico State University. An abstract of the results obtained by Professors W. H. Kersting and W. E. Thompson, aided by Dr. M. Etezadi-Amoli, follows:

"Mathematical models are developed for the steady-state analysis and load-flow studies of ac power systems involving dc transmission lines. A number of typical problems arising out of practical situations are considered and solution of the basic equations of the model is discussed for each problem. A special load-flow program is developed for analyzing ac power systems involving high voltage (superconducting/conventional) dc transmission lines.

Load-flow studies are performed for a projected 'Arizona-New Mexico High Voltage Transmission System.' Results are obtained when the system involves the use of high voltage with superconducting dc lines at selected locations, and performance comparisons are made with the situation where only ac transmission is used as well as where conventional dc transmission is used. These studies indicate that the superconducting dc transmission lines perform quite satisfactorily as far as steady-state behavior is concerned, but no transient or stability studies are considered. In addition to the losslessness of the superconducting dc line, it also requires fewer Mvars than the conventional dc line."

The second phase of the work will deal with the transient analysis of the system.

VI-2. EPRI

A one year contract, awarded by the Electric Power Research Institute (EPRI) effective May 1, will help support the LASL program for developing high T_c, CVD-produced Nb_3Ge. The scope of the contract calls for producing bulk samples on which T_c, I_c, and loss measurements are to be made.

VII. MEETINGS, PRESENTATIONS, MISCELLANEOUS

VII-1. Trips

March 31-April 3. R. J. Bartlett, A. Migliori, W. C. Overton, and R. D. Taylor attended the American Physical Society meeting held in Denver, CO.

April 7-8. R. J. Bartlett discussed dc SPTL with the staff at Iowa State University, Ames, IA.

April 8. M. P. Maley visited Battelle Northwest Laboratories, Richland, WA, and discussed with S. Dahlgren and R. Nelson high rate sputtering capabilities for producing high T_c superconductors.

April 8-9. F. J. Edeskuty, W. E. Keller, and R. D. Taylor visited the Arizona Public Service Company, Phoenix, AZ, toured two substations serving the 238-kV, high-pressure, oil-filled underground cable complex, and discussed cables and dc SPTL with H. V. Taylor, C. Jarman, J. Dustin, J. M. Wiestling, and E. E. Chartier. As a result of this meeting, J. M. Wiestling, Supervising Engineer for Electrical Distribution Engineering and Engineering Services, will regularly visit LASL to participate in the dc SPTL program.

April 15. J. W. Dean and W. F. Stewart visited L. Thompson of Vacuum Barrier Corp., Boston, MA, to discuss cryogenic enclosures.

April 16-17. J. W. Dean and W. F. Stewart visited Brookhaven National Laboratory, Upton, NY, to discuss cryogenic aspects of SPTL designs.

April 18. J. W. Dean and W. F. Stewart discussed the dc SPTL project with B. Belanger, Division of Electric Energy Systems, ERDA, Washington,DC.

April 22. W. E. Keller and R. D. Taylor participated in a program review of the BNL Power Transmission Project at Brookhaven National Laboratory, Upton, NY.

April 23. W. E. Keller and R. D. Taylor discussed LASL proposed research activities in superconductivity with D. Stevens, M. C. Wittels, and L. Ianniello, Division of Physical Research, ERDA, Washington, D.C.

May 6-7. F. J. Edeskuty attended the review of the NBS cryogenic program which is sponsored by DEES-ERDA and participated in a workshop concerned with refrigeration and helium conservation.

May 8. M. P. Maley and L. R. Newkirk participated in the ERDA review of the Westinghouse Electric Co. program to develop Nb_3Ge. The meeting was held in Pittsburgh, PA.

May 9. M. P. Maley visited Intermagnetics General Corp., Guilderland, NY, and discussed high T_c – high J_c optimized Nb_3Sn tapes and multifilamentary Nb_3Sn.

VII-2. Presentations at LASL

Following is a partial listing of visitors to LASL who were briefed on the dc SPTL project during the quarter. Special contributions are noted.

April 2. R. Warren, Westinghouse Research Labs, Pittsburgh, PA.

April 7. T. A. Kitchens, National Science Foundation, Washington, D.C.

April 7. D. Dew-Hughes, Brookhaven National Laboratory and University of Leicester, England.

April 10. N. Shackman, Burndy Corp., Wilton, CT.

April 14. P. Chowdhuri, General Electric Company, Erie, PA.

April 25. E. L. Moore, Rockwell International, Los Angeles, CA.

May 5 – June 30. W. R. Decker, Western New Mexico University, Silver City, participated in the short sample I_c program.

May 11 — June 19. E. R. Lady, University of Michigan, Ann Arbor, MI, consulted with the SPTL cryoengineering section.

May 13. S. F. Mauser, Westinghouse Electric Co., East Pittsburgh, PA.

May 13. F. Kadi, Air Products and Chemicals, Inc., Allentown, PA.

May 15. R. F. Gill, Lakeshore Technical Institute, Cleveland, WI.

May 16. S. A. Manatt and P. G. Wapato, Garrett Corp., Los Angeles, CA.

May 21. H. Barnert, Nuclear Research Center, Jülich, Germany.

May 22-23. J. Wiestling, Arizona Public Service Co., Phoenix, AZ.

May 27-29. D. K. Finnemore, Dept. of Physics, Iowa State University, Ames, IA.

May 28. M. I. Yarymovych, Assistant Administrator for Laboratory and Field Coordination, and V. Garber, ERDA, Washington, D.C., and H. E. Roser, ERDA, Albuquerque Operations Office, Albuquerque, NM.

May 29. M. E. Thout, High Power Laboratory, Westinghouse Electric Co., Pittsburgh, PA.

June 6. R. E. Carter and V. V. Marquez, Air Products and Chemicals Co., Long Beach, CA.

June 6. W. Peschka and C. Carpetis, Institut für Energiewandlung und Elektrische Antriebe, Pfaffenwaldring, Germany.

June 10. W. A. Little, Physics Department, Stanford University, Stanford, CA.

June 11-13. J. M. Wiestling, Arizona Public Service Co., Phoenix, AZ.

June 11-12. E. D. Eich, Power Technologies, Millwood, NY, discussed dc SPTL from a cable engineering viewpoint.

June 13. J. C. Fraser, Hughes Aircraft Corp., Culver City, CA.

June 16. Z. Croitoru, Director of Research, Electricite de France, Clamart, France.

June 16. W. N. Lawless, Cryogenic Division of the National Bureau of Standards, Boulder, CO, gave a seminar on low temperature dielectrics.

June 17-18. F. F. Parry, Division of Electric Energy Systems, ERDA, Washington, D.C.

June 19. H. Bethe, Cornell University, Ithaca, NY.

June 24. R. P. Warren, Martin Marietta Co., Denver, CO.

VII-3. Papers

E. F. Hammel, "Energy and Cryoengineering," Cryogenics 15, 57-63 (1975).

H. L. Laquer, "Superconducting Magnetic Energy Storage," Cryogenics 15, 73-79 (1975).

VII-4. Personnel

Contributors to the work reported (by sections) include the following people: R. J. Bartlett, W. R. Decker, H. L. Laquer, M. P. Maley, R. D. Taylor, and J. Thompson (Sec. II); J. K. Hoffer, E. C. Kerr, and W. L. Willis (Sec. III); J. W. Dean, F. J. Edeskuty, E. R. Lady, and W. F. Stewart (Sec. IV); and J. M. Dickinson and L. Newkirk (Sec. V).

R. V. Carlson, a recent graduate of the University of Minnesota specializing in superconductivity, has joined the dc SPTL project on a post-doctoral appointment. Dick will be primarily concerned with ripple losses determined calorimetrically.

P. Chowdhuri joined the project in June, coming from General Electric Co., Erie, PA. Prit is an Electrical Engineer having received his Ph.D. from Renssalaer Polytechnic Institute and he serves on several IEEE committees. He will be in charge of the power and systems engineering aspects of the dc SPTL.

W. L. Willis has taken a position with the laser-fusion program at LASL.

☆ U.S. GOVERNMENT PRINTING OFFICE: 1975—677-343/67